Excited-State Electronic Asymmetry Prevents Photoswitching in Terthiophene Compounds

Strudwick, B.H.; Zhang, J.; Hilbers, M.F.; Buma, W.J.; Woutersen, S.; Liu, S.H.; Hartl, F.

DOI
10.1021/acs.inorgchem.8b01005

Publication date
2018

Document Version
Final published version

Published in
Inorganic Chemistry

Inorganic Chemistry
Cite This: Inorg. Chem. 2018, 57, 9039−9047
Article
pubs.acs.org/IC

Excited-State Electronic Asymmetry Prevents Photoswitching in Terthiophene Compounds

Benjamin H. Strudwick,*[,†] Jing Zhang,[‡] Michiel F. Hilbers,[†] Wybren Jan Buma,[†] Sander Woutersen,[†] Sheng Hua Liu,[‡] and František Hartl*[,¶]

[†]Molecular Photonics Group, Van 't Hoff Institute for Molecular Sciences, University of Amsterdam, Science Park 904, 1098 XH Amsterdam, The Netherlands

[‡]Key Laboratory of Pesticide and Chemical Biology, Ministry of Education, College of Chemistry, Central China Normal University, Wuhan 430079, P.R. China

[¶]Department of Chemistry, University of Reading, Whiteknights, Reading RG6 6AD, United Kingdom

Supporting Information

ABSTRACT: The diarylethene moiety is one of the most extensively used switches in the field of molecular electronics. Here we report on spectroscopic and quantum chemical studies of two diarylethene-based compounds with a non-C_3-symmetric triethynyl terthiophene core symmetrically substituted with RuCp*(dppe) or trimethylsilyl termini. The ethynyl linkers are strong IR markers that we use in time-resolved vibrational spectroscopic studies to get insight into the character and dynamics of the electronically excited states of these compounds on the picosecond to nanosecond time scale. In combination with electronic transient absorption studies and DFT calculations, our studies show that the conjugation of the non-C_3-symmetric triethynyl terthiophene system in the excited state strongly affects one of the thiophene rings involved in the ring closure. As a result, cyclization of the otherwise photochromic 3,3″-dimethyl-2,2′:3′,2″-terthiophene core is inhibited. Instead, the photoexcited compounds undergo intersystem crossing to a long-lived triplet excited state from which they convert back to the ground state.

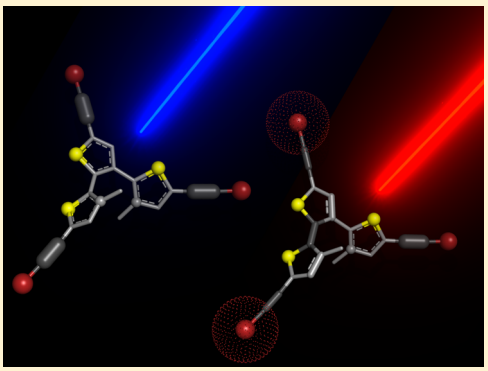

INTRODUCTION

The top-down approach in lithography is rapidly reaching its theoretical limit, with the past decade showing solid-state devices approaching the nanoscale.[1−5] The bottom-up approach, that is fabricating molecular devices capable of imitating macroscopic machinery, is therefore increasingly attracting attention.[6−9] In this bottom-up approach, the reversible photoisomerization reaction of diarylethene that has been studied extensively since the first report in 1988[10] is an often employed component for constructing novel molecular electronic devices.[11−13] Diarylethene-based compounds have proven to be thermally irreversible and resistant to fatigue and to exhibit a highly efficient ring closure, making them prime candidates for electronic switches.[4,11,14,15]

The compounds of interest in this work, **1a** and **1b** shown in Figure 1, have diarylethene cores constructed using a thiophene bridging unit. The thienyl groups are attached at the 2- and 3-positions of the central bridging thiophene ring, Figure 2. Unlike more common bridging units, such as octafluorocyclopentene, diarylmaleic anhydride, or diarylmaleimide,[11,16,17] thiophene has the potential to reduce expenses, due to a more efficient synthesis using less volatile starting materials, which enables the scale up of production.[18] The terthiophene core explored in this research (Figure 2) has demonstrated photocyclization,[18,19] thereby closely following the observation of ring closure in terthiophenes in general[12] with and without substituents on the terthiophene core.[20] However, it should be noted that the literature regularly reports a more commonly used diarylethene structure (1,2-bis(2-methylthiophen-3-yl)ethene) where the positions of the sulfurs differ to the ones presented here. This study utilizes inverse diarylethenes, which have shown ring closure.[21] One of the main reasons for diarylethenes failing to cyclize is a result of the parallel conformation, in which the central methyl groups point in the same direction.[11,22] The addition of bulky groups on the other hand promote the reactive antiparallel form.[23]

The motivation for investigating **1a** and **1b** is an extension of work on dinuclear organometallic-substituted diarylethenes[11,17,23] in which the degree of sophistication of diarylethenes was increased by creating a multifunctional (photo and redox) switch. Ethynyl-bridged metallic complexes have been extensively studied[4,24−27] and found to exhibit electronic properties that are influenced by the metal and the carbon-rich bridges.[26] Dinuclear organometallic compounds

Received: April 17, 2018
Published: July 20, 2018

DOI: 10.1021/acs.inorgchem.8b01005
Inorg. Chem. 2018, 57, 9039−9047

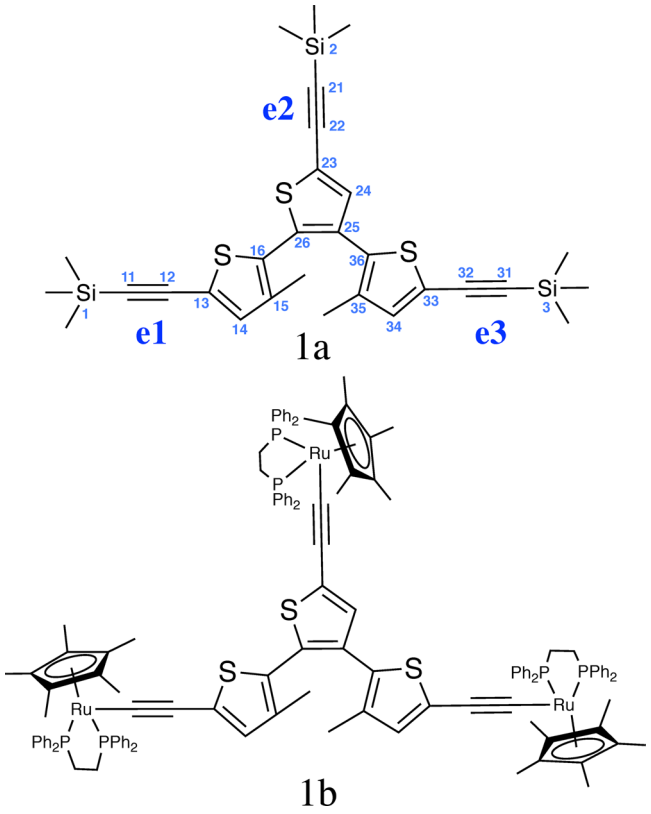

Figure 1. Studied **1a** and **1b** ethynyl-terthiophene compounds terminated with trimethylsilyl (TMS) and RuCp*(dppe), respectively.

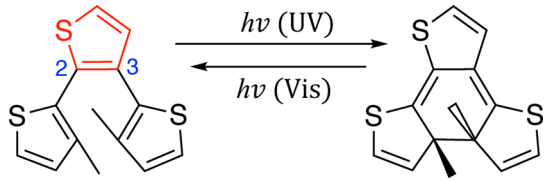

Figure 2. Photochromic reaction of non-C_3-symmetric terthiophene,[18] constructed of diarylethenes with a thiophene-bridging unit (highlighted in red).

have been constructed with central diarylethene and ethynyl-bridged metallic termini.[28] Importantly, these compounds retain their photochromic properties[17,23] but can also be switched electrochemically.[16,17] From this research, further insight was obtained on the electronic communication between the termini in both the open and closed states.

The alignment of a thiophene bridge to diarylethenes allowed for a terthiophene system to be investigated. The electronic and bonding properties of **1a** and **1b** have been previously elucidated by anodic spectro-electrochemistry.[29] Compound **1a** did not show any anodic steps within the accessible potential window nor was there any evidence for photocyclization. Replacing the TMS groups in **1a** with the RuCp*(dppe) termini in **1b** results in the appearance of three consecutive oxidation steps.[29] In the open form of **1b**, it was found that the lateral electrophores do not communicate directly and oxidize independently. In view of previous results[23] that showed that the introduction of ruthenium to the system enhances photocyclization of diarylethene from triplet excited states, ring closure appeared to be an attractive strategy to increase the electronic communication between the electrophores. However, unlike the dinuclear analogs[17,28] UV/vis spectro-electrochemistry of **1b** showed no evidence of cyclization in any of the three anodic steps.[29] Since the 3,3″-dimethyl-2,2′:3′,2″-terthiophene core by itself does show photoreactivity,[18,19] it is key to understand how the highly conjugated ethynyl linkers in these systems inhibit photocyclization, as this will pave the way for developing photoreactive trinuclear systems with a variable degree of electronic communication between the remote termini.

The generally accepted mechanism for cyclization is based on the reversible electrocyclic reaction of the central 6π-electron system.[11,22,30,31] Studies that follow these structural changes in real time have commonly employed UV/vis transient absorption spectroscopy.[32−37] Vibrational spectroscopy has been taken advantage of by using picosecond time-resolved Stokes and anti-Stokes Raman spectroscopy[38] to follow the cyclization mechanism with an experimental temporal resolution of ∼4 ps. However, femtosecond time-resolved UV/vis−IR studies offer a significantly more detailed view on such dynamics[7] but as yet are absent. The ethynyl groups have been demonstrated to be infrared markers that sensitively respond to changes in the oxidation state.[24,29] As will be shown here, time-resolved infrared (TR-IR) spectroscopic studies that target these modes are therefore an ideal means to monitor the changes that occur in the electronic structure upon excitation of the trinuclear non-C_3-symmetric terthiophene compounds of interest. This, in turn, will allow us to determine the underlying reasons for the photostability of these compounds and suggest modifications to enable cyclization.

EXPERIMENTAL METHODS

Synthesis and Sample Preparation. Compounds **1a** and **1b** were synthesized as reported in the literature.[29] Initially, dichloromethane (DCM) dried over 4 Å molecular sieves was used as a solvent. After the discovery of photo-oxidation of **1b** in DCM (see section S1 in SI) anhydrous (≥99.9%), inhibitor-free tetrahydrofuran (THF) purchased from Sigma-Aldrich was used as well as an alternative solvent. In our nanosecond UV/vis transient absorption and time-resolved IR absorption experiments, the solution was pumped through a cell so that fresh sample was probed with each laser shot. This was not possible for the femtosecond UV/vis transient absorption experiments, but in these experiments, steady-state absorption spectra taken before and after the experiments showed no degradation of **1a** in both solvents or of **1b** in THF. The sample concentrations were adjusted to obtain absorbances of 0.8−1 at the pump wavelength (400 nm). All samples were prepared under an inert atmosphere of dry nitrogen. The samples were bubbled with dry argon prior to the measurements. Steady-state UV/vis and IR absorption spectra of **1a** and **1b** are given in the SI, section S2.

Femtoscond Transient Spectroscopy. Time-resolved infrared spectroscopy was performed using commercially available Ti:sapphire lasers (Spectra-Physics Hurricane, 600 μJ, ∼100 fs fwhm, and Coherent, 2 mJ, ∼50 fs fwhm). With the amplified output from these lasers and an optical setup described elsewhere,[39] mid-IR pulses with a duration of 200 fs, a bandwidth of 150 cm^{-1} and an energy of 1−3 μJ were produced. UV-pump pulses at 400 nm with energies of 4 μJ were generated by doubling the amplified 800 nm output with a type II BBO crystal and were delayed by mechanically adjusting the beam path. The UV pump was focused and spatially overlapped with the mid-IR probe, and a temporal resolution of ∼200 fs (fwhm) was determined as described previously.[7] The signals were recorded using an electronically gated amplifier, an Oriel M260i spectrometer, and a 32 pixel MCT detector. The samples, in a flow cell equipped with CaF_2 windows spaced by 1 mm, were placed in the mid-IR focus and

DOI: 10.1021/acs.inorgchem.8b01005
Inorg. Chem. 2018, 57, 9039−9047

pumped through the cell to ensure a fresh sample being measured with each laser shot.

Femtosecond visible transient absorption experiments were performed with the Spectra-Physics Hurricane system mentioned above; 2.5% of the 800 nm fundamental light was used to generate a white-light continuum from 350 to 850 nm by focusing on a CaF_2 plate. The fundamental light used for the white-light generation was passed twice over a delay stage, providing up to 3.6 ns time delay. The sample cell was a 1 mm quartz cuvette. The pump light (400 nm) was created as mentioned above and run at 500 Hz, using a mechanical chopper to produce a nonpumped signal acting as a reference measurement. The spectra were measured using a spectrograph (Shamrock 193i with a 150 lines/mm grating) and a single diode array (Hamamatsu NMOS S3901-512Q) detector. The readout was done using fast electronics (TEC5).

Nanosecond Transient Spectroscopy. Nanosecond transient absorption was measured using an in-house assembled setup described elsewhere.[40] A tunable Nd:YAG-laser system (NT342B, Ekspla) produced the 400 nm pump pulse of 1 mJ that passed through the sample orthogonal to the probe light. The white-light source was a high-stability short-arc xenon flash lamp (FX-1160, Excelitas Technologies) with a modified PS302 controller (EG&G). Transient absorption spectra were measured on a gated intensified CCD camera (PI-MAX3, Princeton Instruments) using a 10 ns gate. The samples were continuously pumped through a 1 cm quartz cuvette so that only fresh samples were measured.

DFT and TD-DFT Calculations. DFT and TD-DFT calculations have been performed with the Gaussian09 software package.[41] Compound **1a** geometry optimization, electronic vertical transitions, and frequency calculations were performed at the B3LYP/6-31G(d) level of theory chosen for its good performance with this type of molecular system.[42−45] Solvent effects (DCM) were included using the Polarizable Continuum Model.[46] DFT and TD-DFT calculations of **1b** have been performed in vacuum at the CAM-B3LYP/LANL2DZ level of theory.[47,48]

RESULTS AND DISCUSSION

To obtain insight into the optically excited state of **1a** and its dynamics, we first performed femto- and nanosecond vis-pump/vis-probe experiments in THF (Figures 3 and 4,

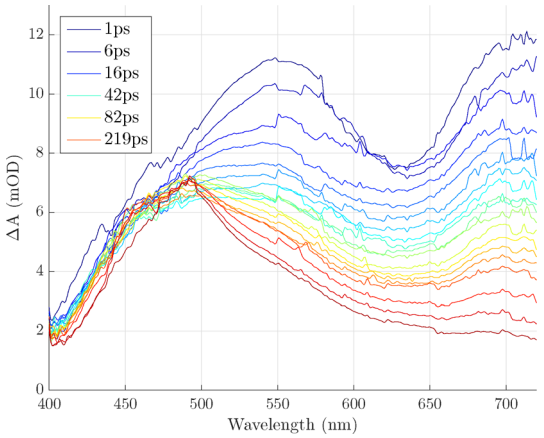

Figure 3. Femtosecond UV/vis transient absorption spectra of **1a** in THF excited at 400 nm. The DAS is shown in the SI, Figure S9.

respectively). Femto- and nanosecond transient spectra were also recorded in DCM (SI, section S3, Figures S7 and S8), with no appreciable difference as compared to THF. In both solvents, **1a** was optically excited with 400 nm photons. TD-DFT calculations of the vertical transitions from the ground state show that the transition with the lowest excitation energy occurs at 3.11 eV (398 nm) with an oscillator strength of f =

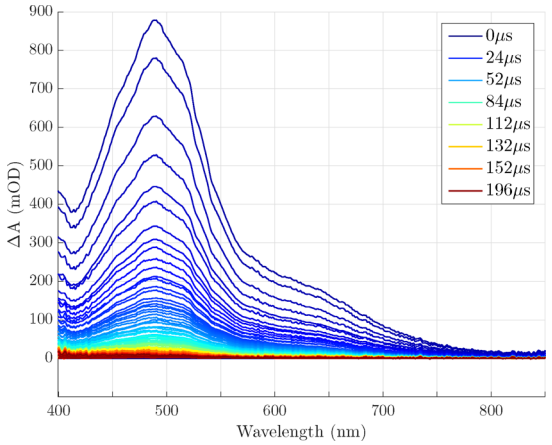

Figure 4. Nanosecond UV/vis transient absorption spectra of **1a** in THF excited at 400 nm.

0.7217 and that it is predominantly described by the HOMO → LUMO (SI, section S4, Figure S10) excitation. The calculated electronic absorption spectrum (SI, section S4, Figure S13) is in good agreement with steady-state UV−vis spectra of **1a** (SI, section S2, Figure S5). In the transient spectra (Figure 3) of **1a**, we can distinguish three spectral features. Initially, within a few picoseconds, a broad feature is seen across the entire spectral window with two distinctive maxima at 550 and 705 nm. From this state, it converts to a second state that is blue-shifted by ca. 25 nm (evident from the decay-associated spectra (DAS) shown in the SI, section S3, Figure S9) but maintains similar spectral features, hinting that the initial state is a hot singlet-excited state. Subsequently a third feature showing a strong absorption at roughly 400−550 nm becomes apparent. This third transient species does not decay within the 4 ns delay range accessible in our femtosecond setup. The transient data matrix for the femtosecond time domain was globally fitted using an open-source program, Gloteran,[49] assuming a sum of exponential time profiles and a sequential model (eq 1):

$$\mathrm{GS} \xrightarrow{h\nu} \mathrm{S}^* \xrightarrow{k_1} \mathrm{S} \xrightarrow{k_2} \mathrm{T} \xrightarrow{k_3} ? \qquad (1)$$

In this model, vertical excitation ($h\nu$) populates a hot singlet state, S*, which is converted into a relaxed singlet state, S, with a time constant of τ_1 = 7 ± 2 ps. The transition from the relaxed singlet state to the triplet state T (as follows from the TR-IR data and TD-DFT calculations discussed below) takes τ_2 = 119 ± 2 ps. The DAS, from the electronic differential absorption measurements, of the S*, S, and T states of **1a** are given in the SI (section S3, Figure S9). In order to further monitor the decay of these electronically excited molecules, nanosecond transient absorption spectra were recorded for **1a** (Figure 4) excited at 400 nm. Singular Value Decomposition (SVD)[50] of the nanosecond transient spectra shows the decay of a single transient species. We have, therefore, using model 2, performed a global analysis of the nanosecond transient data matrix assuming a sum of exponential time profiles and T−T annihilation (described in detail in section S5 in the SI):

$$\mathrm{T} \xrightarrow{k_3} \mathrm{GS} \qquad (2)$$

From these fits, we find a lifetime of the triplet state of τ_3 = 22.7 ± 0.5 μs; fits are shown in Figure 5. The spectral features in the visible region in the nanosecond time domain show no evidence of other transient species, and the long lifetime

DOI: 10.1021/acs.inorgchem.8b01005
Inorg. Chem. 2018, 57, 9039−9047

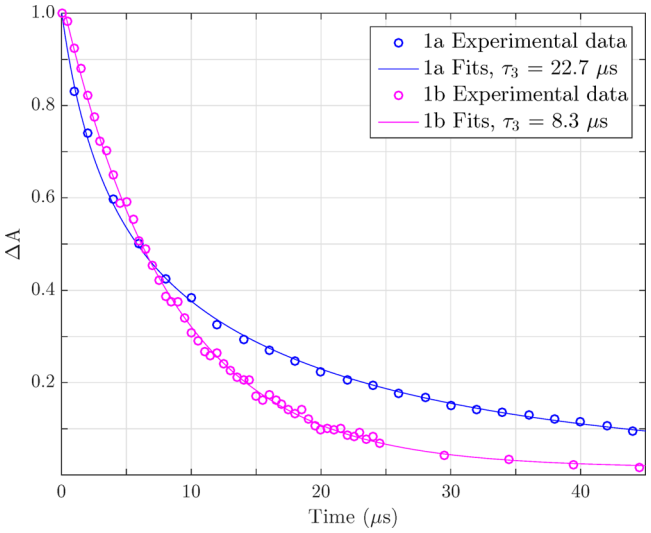

Figure 5. Decay of the transient absorption signal of **1a** (**1b**) at 580 (650) nm in the nanosecond time domain. Spectral absorbances have been normalized.

provides further evidence for triplet-state formation. For aerated solutions, the rate of the T → GS conversion increased for **1a** ($\tau_{3,air}$ = 410 ± 2 ns), again confirming that T is a triplet state.

Complementary TR-IR experiments were performed to obtain a better insight into the electronic structure of each excited state and to determine what inhibits photocyclization of **1a**. The evolution of the TR-IR spectra of **1a** after excitation at 400 nm is shown in Figure 6. Adopting a target model (eq 1), global fits of the TR-IR spectra lead to time constants of τ_1 = 3.0 ± 1 ps and τ_2 = 114 ± 2 ps for **1a**, and the TR-IR decay-associated spectra (TR-IR DAS) that are shown in Figure 6. Comparison of the TR-IR DAS of the initial species (S*) with that of the second species (S) reveals a narrowing of the induced absorption band and its shift to a slightly higher energy of ∼3 cm^{-1}, in line with the conclusion that vibrational cooling of the hot excited singlet state occurs. The femtosecond TR-IR measurements thus confirm that the initial S* state is a hot electronically excited state (note that the TA and TR-IR transients have the same rates of decay). Importantly, neither type of experiment indicates the presence of a ring-closed species. Various parameters such as solvent polarity and excitation wavelength have been changed to see whether under different conditions cyclization might occur, but in all cases no indication was found for cyclization or even a markedly different transient behavior.

Figure 7 shows DFT and TD-DFT predicted IR absorption spectra in the ethynyl stretching region for the ground and excited states of **1a**, with frequencies scaled by 0.95 (which closely follows what is reported in the literature[S1]) and presented in Table 1. Overall good agreement is observed between the experimental and theoretical spectra. Experimentally a ground-state (GS) bleach is observed at 2135 cm^{-1}. The calculations show that this band actually consists of three unresolved bands from the three different stretching modes of the ethynyl linkers. The calculated highest-frequency mode at 2136 cm^{-1} involves mainly the central thiophene ethynyl, labeled e2 in Figure 1. The lower-frequency components at 2132 and 2131 cm^{-1} are assigned to the symmetric and antisymmetric stretching modes of the ethynyl linkers at the lateral thiophenes (e1 and e3 in Figure 1). From the

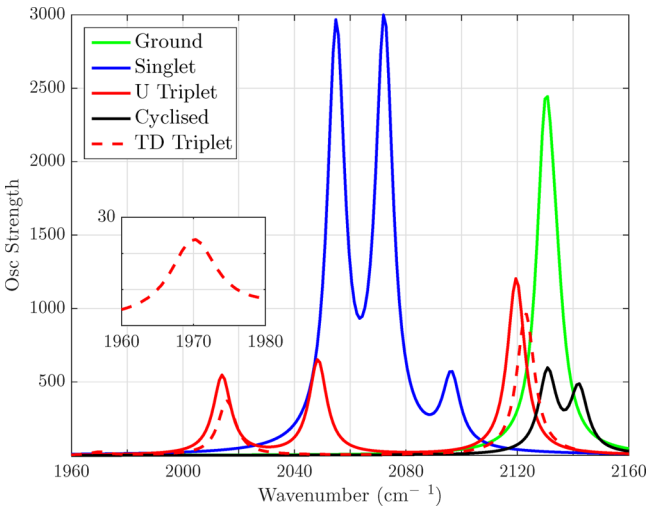

Figure 7. Theoretically predicted IR absorption spectra of the ground state, the lowest excited singlet state, and the lowest excited triplet state of the open form of **1a** as well as of the ground state of its cyclized form. All calculated modes have been broadened to give a fwhm of 4 cm^{-1}.

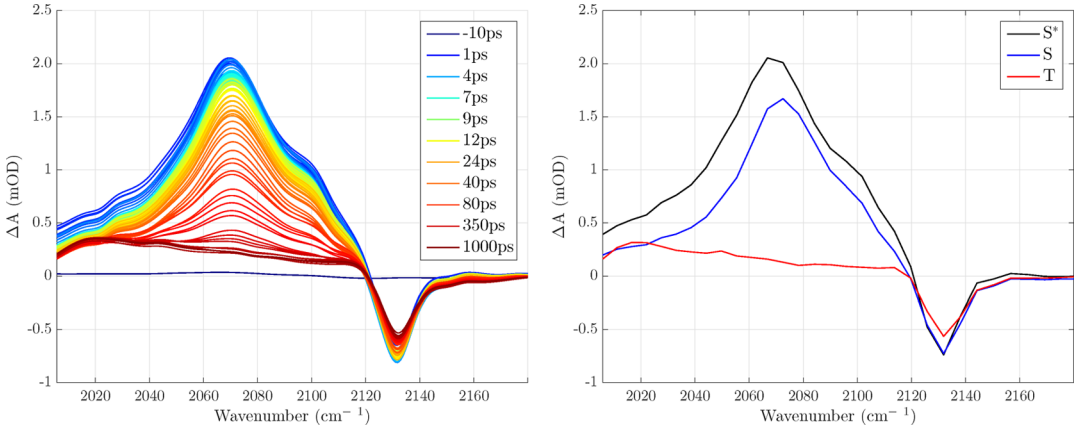

Figure 6. (left) Femtosecond TR-IR spectra of **1a** in DCM and excited at 400 nm. (right) TR-IR decay-associated spectra (DAS) derived from the TR-IR spectra of **1a**.

DOI: 10.1021/acs.inorgchem.8b01005
Inorg. Chem. 2018, 57, 9039−9047

Table 1. Calculated Frequencies of 1a (Scaled by 0.95) and Experimentally Observed Frequencies of 1a and 1b

Calculated Frequencies of **1a** (cm^{-1})					
bond	GS	S	T(TD)	T(U)	cyclized
e1	2132	2054	1969	2014	2141
e2	2136	2074	2015	2048	2129
e3	2131	2095	2122	2119	2142
Measured Frequencies of **1a** and **1b** (cm^{-1})					
bond (compd)		GS	S	T	oxidized
e1 (**1a**)		2135	2069	2019	
e2 (**1a**)			2075	2050	
e3 (**1a**)			2097	2118	
e1 (**1b**)		2050	1936	1936	1935[29]
e2 (**1b**)			1980	1980	1992[29]
e3 (**1b**)			2020	2030	2049[29]

experimentally observed and theoretically predicted small frequency differences one can thus conclude that in the ground state all three linkers are more or less equivalent, and that a complete delocalization of the vibrational excitation occurs over the terthiophene backbone.

This is in marked contrast with the initial singlet excited state (S in Figures 6 and 7), for which there is a lowering of energy of the bands. This is observed in both the experimental and theoretical spectra. The lower energy indicates a weakening of the ethynyl bonds and is in line with what one would expect, but much more surprising is the observation that there are three very distinct bands, since this can only be explained by assuming that the electronic excitation is not equally delocalized over the three linkers. Our calculations show that the main contributions to the experimentally observed absorption bands at 2097, 2075, and 2069 cm^{-1} come from e3, e2 and e1, respectively (Figure 1). These frequency differences nicely follow the changes in bonding character that arise from the HOMO → LUMO transition (SI, section S4, Figure S10), which takes the e1 C≡C from a bonding state in the HOMO to an antibonding state in the LUMO. For the e2, C≡C the antibonding character is less pronounced than for e1, and even less for the e3 C≡C for which the LUMO is almost nonbonding. The asymmetry of the non-C_3-symmetric terthiophene core thus has dramatic consequences for the character of the excitation, which we can now conclude is strongly localized on the e1 thiophene arm and to a lesser extent on the e2 arm and leaves the e3 arm practically unaffected.

TD-DFT calculations have also been performed for the lowest excited triplet state (Figure 7). The agreement between theory and experiment is in this case considerably less than observed above for the lowest excited singlet state. Interestingly, we find that calculations at the unrestricted DFT (U-DFT) level lead to a much better agreement (see Figure 7) indicating that a variational treatment apparently is better able to recover the character of this state than the perturbation approach used in TD-DFT (this has been found to be the case for similar systems in the literature[52−54]). Inspection of the modes calculated at the U-DFT level shows that the mode calculated at 2014 cm^{-1} is associated with the asymmetric stretching mode of e1 and e2 with the major contribution coming from e1. The corresponding symmetric stretching mode with e2 being most involved is found at 2048 cm^{-1}, while the e3 stretching is solely responsible for the IR absorption at 2119 cm^{-1}. The latter mode is not directly apparent in the experimental TR-IR spectra because of its overlap with the GS bleach, but on closer inspection can be found by the shoulder that is visible at about 2110 cm^{-1} and the partial recovery of the GS bleach at a similar rate as the population of the triplet state.

Previously we have concluded that in the lowest excited singlet state the excitation is strongly localized on two of the arms. Comparison of the IR absorption spectra of the lowest excited singlet and triplet states shows that in the lowest triplet state such a localization is even more pronounced. The frequency of the e3 C≡C stretch mode increases with energy with respect to that of the lowest excited singlet state and almost the same as in the ground state while at the same time the absorption bands associated with the e1 and e2 C≡C stretch modes undergo a decrease in energy.

Figure 7 and Table 1 also present DFT-calculated IR absorption bands for the ground state of the hypothetical photocyclized form of **1a**. Here we find symmetric and antisymmetric combinations of e1 and e3 at 2141 and 2142 cm^{-1}, respectively, while the stretch mode of the central e2 ethynyl group is calculated at 2129 cm^{-1}. Despite the lack of experimental evidence for photocyclization, the DFT calculations do not exclude its occurrence. Relative to the GS, the S is 61.3 kcal mol^{-1} higher in energy. The T(U) is calculated to be 42.8 kcal mol^{-1} higher than the GS while the T(TD) predicts it to be 36.5 kcal mol^{-1} higher than the GS. The energy of **1a** is about 35 kcal mol^{-1} higher for the cyclized complex compared to the parent open-triangle form in the GS. Hence, cyclization from the S state or the triplet state (either the U or TD) is energetically feasible; albeit the TD calculated triplet state energy is very close to that of the cyclized compound. Therefore, it is likely there is a high activation barrier in all the excited states that cannot be overcome.

Another possible reason that photoexcitation does not lead to cyclization could be that the methyl groups do not have the appropriate orientation for ring closure to occur. Previous work[11,13] has shown that for the parallel conformer cyclization is inhibited. Although DFT calculations do not show an appreciable energy difference between the two forms, the antiparallel form being a mere 0.1 kcal mol^{-1} lower in energy, NOESY measurements on **1a** (SI, section S6, Figures S15 and S16) provide no evidence for the presence of the parallel conformer in the ground state. Upon excitation, the antiparallel form might convert to the parallel conformer by rotation about one of the bridging bonds, namely $C_{16}-C_{26}$ or $C_{25}-C_{36}$ (Figure 1). SVD[50] in the nanosecond time domain reveals only a single transient species, while the picosecond dynamics can be well explained by vibrational cooling and intersystem crossing to the triplet manifold. The literature, backed up by our NMR measurements (SI, section S6, Figure S17), also rules out *E*/*Z*-isomerization as a possible reason for absence of cyclization, as the bridging thiophene unit prevents the formation of the *E*-form.[13]

The TR-IR measurements backed up by the TD-DFT calculations show that the HOMO has equal contributions from the three arms but that the LUMO resides heavily on the left side of **1a**. These orbitals closely resemble the analogous orbitals found in previous work[29] on a model of **1b**. In line with our conclusions regarding the influence of the asymmetry on the electronic properties, calculations on $\mathbf{1b}^+$ show that in the oxidized form the spin density is asymmetrically distributed, with the largest contributions from the thiophenes involved in the e1 and e2 arms. The asymmetry by itself cannot

DOI: 10.1021/acs.inorgchem.8b01005
Inorg. Chem. 2018, 57, 9039−9047

be the only reason why **1a** does not undergo ring closure, since from previous studies it is known that non-C_3-symmetric terthiophene cores[18,19] can cyclize. In the following, we will argue that the attachment of the ethynyl-based substituents onto the non-C_3-symmetric terthiophene core leads to changes in the conjugation, which in turn are expected to have a major impact on the photocyclization pathway.

Our TR-IR studies show that electronic excitation has a large influence on the bonding properties of the e1 ethynyl linker: instead of the triple bond character it has in the ground state, bonding becomes reduced. The same is true for the e2 ethynyl linker albeit to a lesser extent. In terms of valence bond structures this implies that the contribution of the structure depicted in Figure 8 to the electronic wave function is

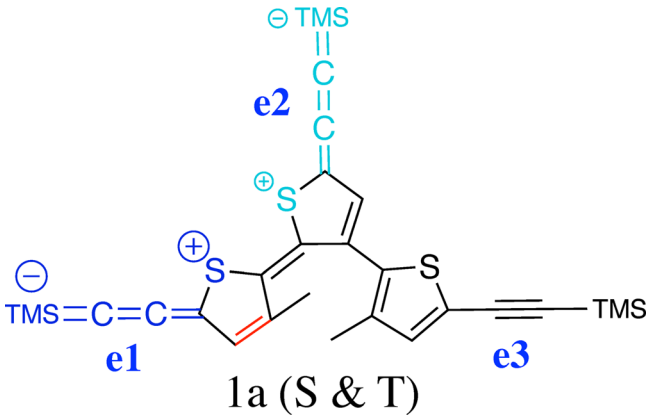

Figure 8. Valence bond structure of **1a** that gains importance in the singlet and triplet excited states. Charge size and color annotated on the arms indicate the degree of charge separation, the e1 arm thus having a larger degree of charge separation than e2.

increased considerably in the electronically excited states. Our observation that in the photoexcited triplet state bonding characters are more reduced than in the photoexcited singlet state demonstrates that in the triplet state this mesomeric structure has an even larger contribution than in the singlet state. This increased contribution has a major impact on the conjugation in both states as becomes clear from the bond lengths reported in Table S1, section S4 of the SI. The calculations show that the e1 and e2 ethynyl bonds $C_{11}-C_{12}$ and $C_{21}-C_{22}$ (numbered in Figure 1) lengthen in both S and T compared to GS, while for the e3 ethynyl bond $C_{31}-C_{32}$, the change in bond length is much smaller. At the same time, they show for the thiophene ring attached to e1 a sizable shortening of the $C_{14}-C_{15}$ bond (a change in the electron density of this bond, from the HOMO to the LUMO, can be clearly seen in the SI section S4, Figure S11) and a lengthening of $C_{13}-C_{14}$ and $C_{15}-C_{16}$ bonds, giving rise to a quasi-inversion of single and double bond character upon excitation. Finally, also the $C_{16}-C_{26}$ bond connecting the e1 and e2 thiophene arms changes from a single into a double bond. Analogous but smaller changes are observed for the e2 arm, while the e3 arm is hardly affected. Cyclization is clearly a highly unfavorable process for the mesomeric structure depicted in Figure 8. In order to cyclize the $C_{13}-C_{14}$ bond, which has been shown to have double bond like characteristics in the excited state (SI, section S4, Figure S11), would have to become unsaturated, having a knock on effect on the conjugation throughout the whole molecule. The increased contribution in the electronically excited states thus provides a logical explanation for the absence of photocyclization in both the singlet and triplet states.

The insight that we have now acquired on the electronic structure of **1a** and how this structure changes upon photoexcitation provides an excellent starting point for assessing the influence of the ruthenium termini in **1b**. Importantly, **1b** also enables us to compare the properties of the photoexcited compound with those of the electrochemically oxidized one, which was not possible for **1a** as electrochemical studies of the latter have not been reported yet. Figure 9 displays nanosecond UV/vis transient absorption

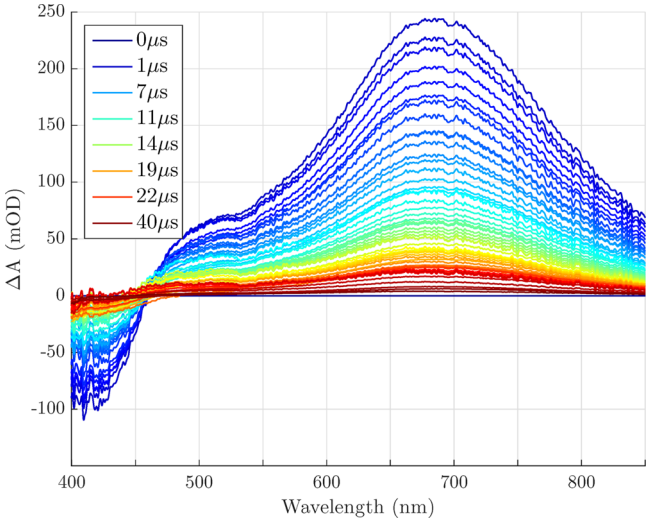

Figure 9. Nanosecond UV/vis transient absorption spectra of **1b** in THF excited at 400 nm.

spectra of **1b**. Nanosecond UV/vis transient absorption experiments show that photoexcitation of **1b** in THF eventually populates the triplet state T (Figure 9). As a result of the ruthenium termini absorption from T now occurs at ca. 650 nm and is thus strongly red-shifted from the ca. 480 nm absorption observed for **1a**. Global analysis of these data using model S1 (SI, section S5) that assumes a sum of exponential time profiles and triplet−triplet annihilation lead to a time constant τ_3 = 8.3 ± 0.5 μs for the T → GS decay, which is a factor three faster than that observed for **1a**; fits are shown in Figure 5. This increase in decay rate is not surprising in view of the increased spin−orbit coupling in **1b** due to the Ru atoms. Femtosecond UV/vis transient absorption spectra of **1b** (SI, section S7, Figure S18) show that the triplet state is populated within the first 20 ps but do not provide a clear view on the early time dynamics.

Previously, it has been shown that attachment of the ethynyl-metal based substituents onto a symmetric terthiophene core does not impede cyclization.[17] In the present experiments, in contrast, we do not observe any evidence for cyclization. In fact, from the full recovery of the GS bleach in Figure 9, it can be concluded that in THF **1b** completely reverts back to the GS.

TR-IR spectra of **1b** are shown in Figure 10. Global analysis of these spectra gives rise to two species with DAS that are displayed in Figure 10. The final species can clearly be associated with T, which is populated with a time constant of τ_2 = 5 ± 2 ps. This is considerably faster than what is observed for **1a** but entirely in line with the strong spin−orbit coupling

DOI: 10.1021/acs.inorgchem.8b01005
Inorg. Chem. 2018, 57, 9039−9047

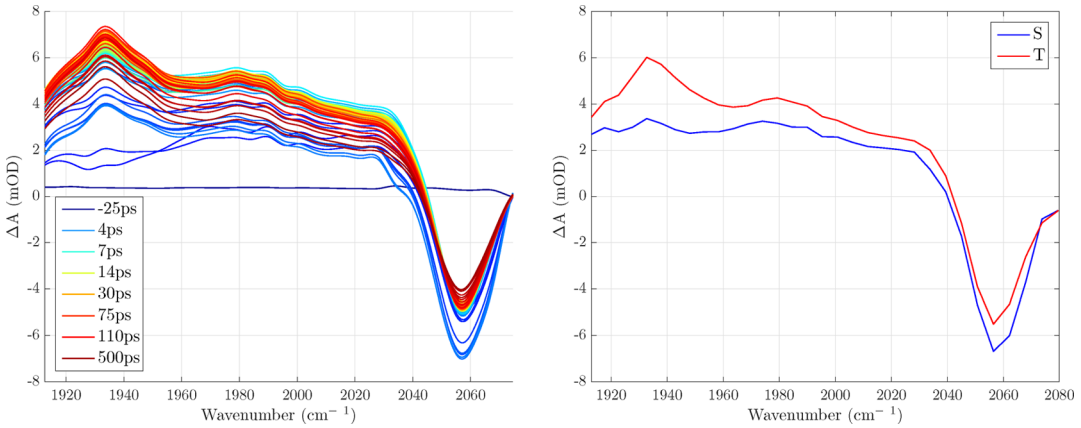

Figure 10. (left) Femtosecond TR-IR spectra of **1b** in THF excited at 400 nm. (right) TR-IR decay-associated spectra (DAS) of **1b**.

due to the presence of the Ru atoms[23] that was previously concluded to be responsible for the increased decay rate of the triplet to the ground state. The assignment of the first species, on the other hand, is not directly clear. It could be associated with the initially excited singlet state, but this would imply that the excited singlet and triplet states have very similar ethynyl stretch frequencies, which in view of our observations for **1a** where distinct IR absorption spectra were observed for both states would not directly be expected. Alternatively, the narrowing of the bands in the DAS of the second species as compared to those in the first species and the decay rate of the first species would be in line with a vibrational cooling process occurring in the triplet manifold. In that case intersystem crossing would be faster than the ∼1 ps time resolution of our TR-IR experiments.

Comparison of the ethynyl vibrational characteristics of **1a** and **1b** shows that in the ground state of **1b** frequencies are reduced by about 100 cm^{-1}, indicating delocalization of the conjugation over the Ru termini; this is backed up by the HOMO plot of **1b** in the SI section 4 (Figure S12). However, in the triplet state the ethynyl modes undergo the same asymmetric frequency shifts in **1b** as in **1a** as can be concluded from Table 1. We thus conclude that in both compounds electronic excitation leads to very similar changes in the electronic structure, and in particular to an increase of the contribution of the mesomeric structure shown in Figure 8. In section S4 (Figure S12) of the SI the LUMO+1 of **1b** is presented. The calculations of the 10 lowest energy vertical transitions are presented in the SI section S4 (Figure S14), which reveal one dominant transition associated with the HOMO → LUMO+1 transition. The comparison of the LUMO of **1a** and the LUMO+1 of **1b** confirms the similarities between the excited states, especially when the LUMO/LUMO+1 on the C_{14}−C_{15} bond of the two compounds are compared. It would therefore appear that modifying the arms with the Ru termini, aiming thereby to change the asymmetry in the character of the electronically excited states as well, does not change the conjugation to such an extent that cyclization becomes possible.

Interestingly, we find that the changes in the ethynyl frequencies in the triplet state of **1b** closely follow the changes when **1b** is oxidized (Table 1).[29] The asymmetry in the electronic wave function of $\mathbf{1b}^+$ is further supported by the spin density distribution, which is found to reside heavily on the lateral side of $\mathbf{1b}^+$ between e1 and e2. Moreover, the electronic absorption spectrum from the triplet state of **1b** and the ground state of $\mathbf{1b}^+$ show similar features, both having strong absorption bands with maxima at ca. 730 nm for $\mathbf{1b}^+$ (SI, section S1 (Figure S3)) and ca. 680 nm for the T state (Figure 9). These spectroscopic markers thus indicate that **1b** in its lowest excited triplet state is similar to the ground state of the one-electron oxidized form. This suggests that the photo-induced promotion of an electron from the HOMO to the antibonding LUMO (**1a**)/LUMO+1 (**1b**) and the complete electrochemical removal of an electron from the HOMO both result in a similar weakening of the e1 and e2 ethynyl characteristics and modified conjugation in the terthiophene core.

CONCLUSIONS

To summarize, we have investigated two open-triangle triethynyl terthiophene compounds, **1a** and **1b**, that show a surprising photostability instead of switchable photocyclization. Visible transient spectroscopy has unveiled the decay pathways of both compounds that populate the triplet state manifold. Using the ethynyl groups as sensitive IR markers for the electronic structure of these compounds in ground and electronically excited states, we have shown that in both compounds electronic excitation induces an electronic asymmetry in the terthiophene core. The concurrent reduction of electronic delocalization has far-reaching consequences, as it increases the importance of mesomeric structures that do not favor cyclization, as is indeed observed. Although the addition of the Ru termini extends delocalization of the electronic wave function in the ground state, it does not modify the electronic structure of the electronically excited states as to enable cyclization.

The present study has revealed what prevents photocyclization in these asymmetric terthiophene compounds. It thereby provides a solid starting point for designing novel compounds in which asymmetry could be compatible with gating electron and energy transfer using photocyclization and electrochemistry. Such studies are presently underway.

ASSOCIATED CONTENT

Supporting Information

The Supporting Information is available free of charge on the ACS Publications website at DOI: 10.1021/acs.inorgchem.8b01005.

Photo-oxidation of **1b** in DCM monitored by FT-IR and UV/vis spectroscopy; IR and UV/vis absorption spectra

DOI: 10.1021/acs.inorgchem.8b01005
Inorg. Chem. 2018, 57, 9039−9047

of **1a** and **1b**; UV/vis transient absorption spectra of **1a**; DFT and TD-DFT calculations of **1a** and **1b**; global fitting of nanosecond transient absorption spectra (the model); proton NMR and NOESY spectra of **1a**; femtosecond transient spectra of **1b** in THF in the visible region (PDF)

AUTHOR INFORMATION

Corresponding Authors

*E-mail: b.h.strudwick@uva.nl.
*E-mail: f.hartl@reading.ac.uk.

ORCID

Sander Woutersen: 0000-0003-4661-7738
František Hartl: 0000-0002-7013-5360

Notes

The authors declare no competing financial interest.

ACKNOWLEDGMENTS

Author S.W. kindly acknowledges the John van Geuns Foundation for financial support. Authors J.Z., S.H.L., and F.H. gratefully acknowledge financial support from the National Natural Science Foundation of China (21472059), the Overseas Talent Plan 111 Project B17019. This work was supported by the Nederlandse Organisatie voor Wetenschappelijk Onderzoek (NWO).

REFERENCES

(1) Carroll, R. L.; Gorman, C. B. The Genesis of Molecular Electronics. *Angew. Chem., Int. Ed.* **2002**, *41*, 4378−4400.
(2) Joachim, C.; Gimzewski, J. K.; Aviram, A. Electronics using hybrid-molecular and mono-molecular devices. *Nature* **2000**, *408*, 541−548.
(3) Low, P. J. Metal complexes in molecular electronics: progress and possibilities. *Dalton Trans.* **2005**, 2821−2824.
(4) Xiang, D.; Wang, X.; Jia, C.; Lee, T.; Guo, X. Molecular-Scale Electronics: From Concept to Function. *Chem. Rev.* **2016**, *116*, 4318−4440.
(5) Lörtscher, E. Wiring molecules into circuits. *Nat. Nanotechnol.* **2013**, *8*, 381−384.
(6) Panman, M. R.; Bodis, P.; Shaw, D. J.; Bakker, B. H.; Newton, A. C.; Kay, E. R.; Leigh, D. A.; Buma, W. J.; Brouwer, A. M.; Woutersen, S. Operation Mechanism of a Molecular Machine Revealed Using Time- Resolved Vibrational Spectroscopy. *Science* **2010**, *328*, 1255−1258.
(7) Panman, M. R.; Bodis, P.; Shaw, D. J.; Bakker, B. H.; Newton, A. C.; Kay, E. R.; Leigh, D. A.; Buma, W. J.; Brouwer, A. M.; Woutersen, S. Time-resolved vibrational spectroscopy of a molecular shuttle. *Phys. Chem. Chem. Phys.* **2012**, *14*, 1865−1875.
(8) Bissell, R. A.; Córdova, E.; Kaifer, A. E.; Stoddart, J. F. A chemically and electro-chemically switchable molecular shuttle. *Nature* **1994**, *369*, 133−136.
(9) Brouwer, A. M.; Frochot, C.; Gatti, F. G.; Leigh, D. A.; Mottier, L.; Paolucci, F.; Roffia, S.; Wurpel, G. W. H. Photoinduction of Fast, Reversible Translational Motion in a Hydrogen-Bonded Molecular Shuttle. *Science* **2001**, *291*, 2124−2128.
(10) Nakamura, S.; Irie, M. Thermally irreversible photochromic systems. A theoretical study. *J. Org. Chem.* **1988**, *53*, 6136−6138.
(11) Irie, M.; Fukaminato, T.; Matsuda, K.; Kobatake, S. Photochromism of diarylethene molecules and crystals: Memories, switches, and actuators. *Chem. Rev.* **2014**, *114*, 12174−12277.
(12) Jayasuriya, N.; Kagan, J.; Owens, J. E.; Kornak, E. P.; Perrine, D. M. Photocyclization of terthiophenes. *J. Org. Chem.* **1989**, *54*, 4203−4205.
(13) Takeshita, M.; Hirowatari, T.; Takedomi, A. E/Z isomerization of a thermally bistable photochromic dithienylethene. *Tetrahedron Lett.* **2016**, *57*, 3565−3567.
(14) Wang, R.; Ding, H.; Pu, S.; Xia, H.; Liu, G. Syntheses, photochromism and polarization optical recording of a novel diarylethene having a thiazole unit. *International Congress on Image and Signal Processing* **2010**, 2849−2852.
(15) Ishibashi, Y.; Umesato, T.; Fujiwara, M.; Une, K.; Yoneda, Y.; Sotome, H.; Katayama, T.; Kobatake, S.; Asahi, T.; Irie, M.; Miyasaka, H. Solvent Polarity Dependance of Photochromic Reactions of a Diarylethene Derivative As Revealed by Steady-State and Transient Spectroscopies. *J. Phys. Chem. C* **2016**, *120*, 1170−1177.
(16) Motoyama, K.; Li, H.; Koike, T.; Hatakeyama, M.; Yokojima, S.; Nakamura, S.; Akita, M. Photo- and electro-chromic organometallics with dithienylethene (DTE) linker, L_2CpM-DTE-$MCpL_2$: Dually stimuli-responsive molecular switch. *Dalton Trans.* **2011**, *40*, 10643.
(17) Liu, Y.; Lagrost, C.; Costuas, K.; Tchouar, N.; Le Bozec, H.; Rigaut, S. A multifunctional organometallic switch which carbon-rich ruthenium and diarylethene units. *Chem. Commun.* **2008**, *109*, 6117−6119.
(18) Li, X.; Tian, H. One-step synthesis and photochromic properties of a stable triangle terthiophene. *Tetrahedron Lett.* **2005**, *46*, 5409−5412.
(19) Li, X.; Ma, Y.; Wang, B.; Li, G. Lock and key control" of photochromic reactivity by controlling the oxidation/reduction state. *Org. Lett.* **2008**, *10*, 3639−3642.
(20) Kawai, T.; Iseda, T.; Irie, M. Photochromism of triangle terthiophene derivatives as molecular re-router. *Chem. Commun.* **2004**, 72−73.
(21) Wang, J.; Gao, Y.; Zhang, J.; Tian, H. Invisible photochromism and optical anti-counterfeiting based on DA type inverse diarylethene. *J. Mater. Chem. C* **2017**, *5*, 4571−4577.
(22) Erko, F. G.; Berthet, J.; Patra, A.; Guillot, R.; Nakatani, K.; Métivier, R.; Delbaere, S. Spectral, Conformational and Photochemical Analyses of Photochromic Revisited. *Eur. J. Org. Chem.* **2013**, *2013*, 7809−7814.
(23) Jukes, R. T. F.; Adamo, V.; Hartl, F.; Belser, P.; De Cola, L. Photochromic Dithienylethene Derivatives Containing Ru(II) or Os(II) Metal Units. Sensitized Photocyclization from a Triplet State. *Inorg. Chem.* **2004**, *43*, 2779−2792.
(24) Fox, M. A.; Roberts, R. L.; Baines, T. E.; Le Guennic, B.; Halet, J.-F.; Hartl, F.; Yufit, D. S.; Albesa-Jové, D.; Howard, J. A. K.; Low, P. J. Ruthenium complexes of C,C'-bis(ethynyl)carboranes: An investigation of electronic interactions mediated by spherical pseudo-armatic spacers. *J. Am. Chem. Soc.* **2008**, *130*, 3566−3578.
(25) Fitzgerald, E. C.; Ladjarafi, A.; Brown, N. J.; Collison, D.; Costuas, K.; Edge, R.; Halet, J.-F.; Justaud, F.; Low, P. J.; Meghezzi, H.; Roisnel, T.; Whiteley, M. W.; Lapinte, C. Spectroscopic Evidence for Redox Isomerism in the 1,4-Diethynylbenzene-Bridged Heterobimetallic Cation $[\{Fe(dppe)Cp^*\}(\mu\text{-}C{\equiv}CC_6H_4C{\equiv}C)\{Mo(dppe)(\eta\text{-}C_7H_7)\}]PF_6$. *Organometallics* **2011**, *30*, 4180−4195.
(26) Bruce, M. I.; Costuas, K.; Davin, T.; Ellis, B. G.; Halet, J.-F.; Lapinte, C.; Low, P. J.; Smith, M. E.; Skelton, B. W.; Toupet, L.; White, A. H. Iron versus Ruthenium: Dramatic Changes in Electronic Structure Result from Replacement of One Fe by Ru in $[\{Cp^*(dppe)Fe\}\text{-}CC\text{-}CC\text{-}\{Fe(dppe)Cp^*\}]^{n+}$ (n = 0, 1, 2). *Organometallics* **2005**, *24*, 3864−3881.
(27) Steed, J.; Atwood, J. L. *Supramolecular Chemistry*; Wiley: Chichester, 2000.
(28) Hervault, Y.-M.; Ndiaye, C. M.; Norel, L.; Lagrost, C.; Rigaut, S. Controlling the Stepwise Closing of Identical DTE Photochromic Units with Electrochemical and Optical Stimuli. *Org. Lett.* **2012**, *14*, 4454−4457.
(29) Zhang, J.; Sun, C.-F.; Zhang, M.-X.; Hartl, F.; Yin, J.; Yu, G.-A.; Rao, L.; Liu, S. H. Asymmetric oxidation of vinyl- and ethynyl terthiophene ligans in triruthenium complexes. *Dalton Trans.* **2016**, *45*, 768−782.

DOI: 10.1021/acs.inorgchem.8b01005
Inorg. Chem. 2018, 57, 9039−9047

(30) Peters, A.; Mcdonald, R.; Branda, N. R. Regulating π − conjugated pathways using a photochromic 1,2-dithienylcyclopentene. *Chem. Commun.* **2002**, 2274−2275.
(31) Woodward, R. B.; Hoffmann, R. H. *The Conservation of Orbital Symmetry*; Verlag Chemie, 1970.
(32) Lambert, C.; Moos, M.; Schmiedel, A.; Holzapfel, M.; Schäfer, J.; Kess, M.; Engel, V. How fast is optically induced electron transfer in organic mixed valence system? *Phys. Chem. Chem. Phys.* **2016**, *18*, 19405−19411.
(33) Paa, W.; Yang, J.-P.; Helbig, M.; Hein, J.; Rentsch, S. Femtosecond time-resolved measurements of terthiophene: fast singlet -triplet intersystem crossing. *Chem. Phys. Lett.* **1998**, *292*, 607−614.
(34) Ishibashi, Y.; Mukaida, M.; Falkenström, M.; Miyasaka, H.; Kobatake, S.; Irie, M. One-and multi-photon cycloreversion reaction dynamics of diarylethene derivative with asymmetrical structure, as revealed by ultrafast laser spectroscopy. *Phys. Chem. Chem. Phys.* **2009**, *11*, 2640−2648.
(35) Ishibashi, Y.; Umesato, T.; Kobatake, S.; Irie, M.; Miyasaka, H. Femtosecond Laser Photolysis Studies on Temperature Dependence of Cyclization and Cycloreversion Reactions of a Photochromic Diarylethene Derivative. *J. Phys. Chem. C* **2012**, *116*, 4862−4869.
(36) Miyasaka, H.; Araki, S.; Tabata, A.; Nobuto, T.; Malaga, N.; Irie, M. Picosecond laser photolysis studies on photochromic reactions of 1,2-bis (2,4,5-trimethyl-3-thienyl) maleic anhydride in solutions. *Chem. Phys. Lett.* **1994**, *230*, 249−254.
(37) Tamai, N.; Saika, T.; Shimidzu, T.; Irie, M. Femtosecond Dynamics of a Thiophene Oligomer with a Photoswitch by Transient Absorption Spectroscopy. *J. Phys. Chem.* **1996**, *100*, 4689−4692.
(38) Okabe, C.; Nakabayashi, T.; Nishi, N.; Fukaminato, T.; Kawai, T.; Irie, M.; Sekiya, H. Picosecond Time-Resolved Stokes and Anti-Stokes Raman Studies on the Photochromic reactions of Diarylethene Derivatives. *J. Phys. Chem. A* **2003**, *107*, 5384−5390.
(39) Huerta-Viga, A.; Shaw, D. J.; Woutersen, S. pH Dependence of the Conformation of Small Peptides Investigated with Two-Dimensional Vibrational Spectroscopy. *J. Phys. Chem. B* **2010**, *114*, 15212−15220.
(40) Limburg, B.; Hilbers, M.; Brouwer, A. M.; Bouwman, E.; Bonnet, S. The Effect of Liposomes on the Kinetics and Mechanism of the Photocatalytic Reduction of 5,5-Dithiobis(2-Nitrobenzoic Acid) by Triethanolamine. *J. Phys. Chem. B* **2016**, *120*, 12850−12862.
(41) Frisch, M. J.; Trucks, G. W.; Schlegel, H. B.; Scuseria, G. E.; Robb, M. A.; Cheeseman, J. R.; Scalmani, G.; Barone, V.; Mennucci, B.; Petersson, G. A.; Nakatsuji, H.; Caricato, M.; Li, X.; Hratchian, H. P.; Izmaylov, A. F.; Bloino, J.; Zheng, G.; Sonnenberg, J. L.; Hada, M.; Ehara, M.; Toyota, K.; Fukuda, R.; Hasegawa, J.; Ishida, M.; Nakajima, T.; Honda, Y.; Kitao, O.; Nakai, H.; Vreven, T.; Montgomery, J. A., Jr.; Peralta, J. E.; Ogliaro, F.; Bearpark, M.; Heyd, J. J.; Brothers, E.; Kudin, K. N.; Staroverov, V. N.; Kobayashi, R.; Normand, J.; Raghavachari, K.; Rendell, A.; Burant, J. C.; Iyengar, S. S.; Tomasi, J.; Cossi, M.; Rega, N.; Millam, J. M.; Klene, M.; Knox, J. E.; Cross, J. B.; Bakken, V.; Adamo, C.; Jaramillo, J.; Gomperts, R.; Stratmann, R. E.; Yazyev, O.; Austin, A. J.; Cammi, R.; Pomelli, C.; Ochterski, J. W.; Martin, R. L.; Morokuma, K.; Zakrzewski, V. G.; Voth, G. A.; Salvador, P.; Dannenberg, J. J.; Dapprich, S.; Daniels, A. D.; Farkas, O.; Foresman, J. B.; Ortiz, J. V.; Cioslowski, J.; Fox, D. J. *Gaussian 09*, revision D.01; Gaussian, Inc.: Wallingford, CT, 2009.
(42) Tachikawa, H.; Kawabata, H.; Ishida, K.; Matsushige, K. A DFT and direct MO dynamics study on the structures and electronic states of phenyl-capped terthiophene. *J. Organomet. Chem.* **2005**, *690*, 2895−2904.
(43) Higashiguchi, K.; Matsuda, K.; Asano, Y.; Murakami, A.; Nakamura, S.; Irie, M. Photochromism of Dithienylethenes Containing Fluorinated Thiophene Rings. *Eur. J. Org. Chem.* **2005**, *2005*, 91−97.
(44) Al-Anber, M.; Milde, B.; Alhalasah, W.; Lang, H.; Holze, R. Electrochemical and DFT-studies of substituted thiophenes. *Electrochim. Acta* **2008**, *53*, 6038−6047.
(45) Gordon, K. C.; Clarke, T. M.; Officer, D. L.; Hall, S. B.; Collis, G. E.; Burrell, A. K. Vibrational spectra and calculations on substituted terthiophenes. *Synth. Met.* **2003**, *137*, 1367−1368.
(46) Tomasi, J.; Mennucci, B.; Cammi, R. Quantum Mechanical Continuum Solvation Models. *Chem. Rev.* **2005**, *105*, 2999−3094.
(47) Yanai, T.; Tew, D. P.; Handy, N. C. A new hybrid exchange-correlation functional using the Coulomb-attenuating method (CAM-B3LYP). *Chem. Phys. Lett.* **2004**, *393*, 51−57.
(48) Hay, P. J.; Wadt, W. R. Ab initio effective core potentials for molecular calculations. Potentials for K to Au including the outermost core orbitals. *J. Chem. Phys.* **1985**, *82*, 299−310.
(49) Snellenburg, J. J.; Laptenok, S. P.; Seger, R.; Mullen, K. M.; van Stokkum, I. H. M. Glotaran: a Java-based Graphical User Interface for the R-package TIMP. *J. Stat. Softw.* **2012**, *49*, 1−22.
(50) Henry, E. R. The use of matrix methods in the modeling of spectroscopic data sets. *Biophys. J.* **1997**, *72*, 652−73.
(51) Scott, A. P.; Radom, L. Harmonic Vibrational Frequencies: An Evaluation of Hartree-Fock, Møller-Plesset, Quadratic Configuration Interaction, Density Functional Theory, and Semiempirical Scale Factors. *J. Phys. Chem.* **1996**, *100*, 16502−16513.
(52) Gao, Y.; Liu, C.-G.; Jiang, Y.-S. Electronic Structure of Thiophene Oligomer Dications: An Alternative Interpretation from the Spin-Unrestricted DFT Study. *J. Phys. Chem. A* **2002**, *106*, 5380−5384.
(53) Irle, S.; Lischka, H. An ab initio investigation of the charge-transfer complexes of alkali atoms with oligo (α, α') thiophenes and oligoparaphenylenes: A model calculation on polaronic and bipolaronic defect structures. *J. Chem. Phys.* **1995**, *103*, 1508−1522.
(54) Irle, S.; Lischka, H. Combined ab initio and density functionaly study on polaron to bipolaron transitions in oligophenyls and oligothiophenes. *J. Chem. Phys.* **1997**, *107*, 3021−3031.

DOI: 10.1021/acs.inorgchem.8b01005
Inorg. Chem. 2018, 57, 9039−9047